The Canadian Mineralogist
Vol. 35, pp. 1311-1323 (1997)

VOLUME–COMPOSITION RELATIONS IN CONCENTRICALLY ZONED CRYSTALS: APPLICATION TO THERMODYNAMIC MODELING OF IGNEOUS PROCESSES*

JAMES NICHOLLS[1], MAVIS Z. STOUT, JOHN MACHACEK AND PAT MICHAEL

Department of Geology and Geophysics, University of Calgary, Calgary, Alberta T2N 1N4

ABSTRACT

Measured amounts of the compositional ranges of solid solutions in zoned crystals compared to predicted volumes can be used to test the validity of thermodynamic models. Problems associated with estimating modes of zoned crystals include automating the collection of analytical values on zoned crystals and evaluating the error in the estimation of the modal value. The electron microprobe can be programmed to provide precise, simultaneous estimates of the compositions of zoned minerals and the areas of compositional zones exposed on the surface of a thin section. With 10-second counting times on spots automatically located on a grid, typical precisions (1 σ, mol %) are: 0.32% Fa, 0.34% Fo, 0.24% An, and 0.63% Ab. Predicted and measured volumes are compared using relative cumulative frequency curves. The shapes of these curves depend on conditions of crystallization such as pressure, H_2O content, and oxygen fugacity. The relative cumulative frequency curves for spots collected on three olivine phenocrysts and four feldspar phenocrysts from the Nisga'a flow of northern British Columbia show marked differences from those predicted from fractional crystallization models. An analysis of the effects of concentric zoning on the estimation of fractional volumes from fractional areas in central sections through crystals shows that: 1) the areas of outer shells will underestimate the volumes of the shells, 2) the fractional areas of inner shells overestimate the fractional volumes of the shells, 3) the maximum error of estimation, as a percentage of the total volume of the crystal, is approximately 15% as a worst case, and the error can reach the maximum possible only if the shell has both a particular location and thickness, 4) the systematic errors that arise from estimating fractional volumes from fractional areas in section decrease with decreasing thickness of shells, and 5) shells that have widths centered approximately two-thirds of the distance from the center to edge of the crystal will have minimal (~0%) systematic error in their estimated volumes.

Keywords: point counting, systematic errors, mineral analysis, basalt, Nisga'a flow, British Columbia, electron-microprobe analysis, thermodynamic modeling, compositional zoning.

SOMMAIRE

Les intervalles de composition mesurés dans les cristaux zonés d'espèces montrant une solution solide sont comparés avec les volumes prédits afin d'évaluer la validité de modèles thermodynamiques. Il y a des problèmes associés à l'évaluation de la proportion modale de cristaux zonés, dont la collection automatisée de données analytiques pour caractériser les cristaux zonés et l'évaluation de l'erreur associée avec l'analyse modale d'une roche. On peut programmer une microsonde électronique pour produire des estimés précis, de façon simultanée, de la composition de minéraux zonés et de l'aire des zones compositionnelles affleurant à la surface d'une lame mince. Avec des durées de comptage de dix secondes aux endroits automatiquement repérés selon une grille, les précisions typiques (1σ, pourcentages molaires) seraient: 0.32% Fa, 0.34% Fo, 0.24% An, et 0.63% Ab. Les volumes prédits et mesurés sont comparés au moyen de courbes de fréquence cumulative. La forme de ces courbes dépend de conditions de cristallisation, par exemple pression, teneur en H_2O, et fugacité d'oxygène. Les courbes de fréquence cumulative relative pour les résultats d'analyses ponctuelles prélevées sur trois cristaux d'olivine et quatre cristaux de feldspath de la coulée de Nisga'a, dans le nord de la Colombie-Britannique, montrent des écarts importants des courbes prédites selon les modèles de cristallisation fractionnée. Selon notre analyse des conséquences de la cristallisation fractionnée sur l'évaluation des volumes fractionnels de couches de croissance, dérivés des aires fractionnelles mesurées sur des coupes passant par le centre des cristaux, il semble que: 1) l'aire des couches externes sous-estime le volume de ces couches, 2) l'aire fractionnelle des couches internes surestime le volume fractionnel de ces couches, 3) l'erreur maximale de l'estimé, exprimé comme pourcentage du volume total d'un cristal, serait d'environ 15% dans le pire des cas, là où la couche possède à la fois une location et une épaisseur particulières, 4) les erreurs systématiques associées à l'estimation de volumes fractionnels à partir des aires fractionnelles dans une section diminue à mesure que diminue l'épaisseur d'une couche, 5) les couches dont la largeur est centrée environ deux-tiers de la distance du centre vers la périphérie devraient avoir une erreur systématique minime (~0%) dans le volume estimé.

(Traduit par la Rédaction)

Mots-clés: analyse modale, erreurs systématiques, analyse de minéraux, basalte, coulée de Nisga'a, Colombie-Britannique, analyse à la microsonde électronique, modèle thermodynamique, zonation en composition.

* LITHOPROBE contribution number 858.

[1] *E-mail address*: nicholls@geo.ucalgary.ca

INTRODUCTION

Thermodynamic modeling of magmatic processes can predict possible paths of magmatic crystallization. A central issue is a comparison of features in the rock with features predicted by the model, to determine whether the rock actually formed by following the predicted path of crystallization. Features that can be compared include the phases that crystallize, their order of crystallization, and their compositions. These calculations build a continuing chain of process-dependent predictions, and these predictions can be used to test the validity of the models. If the predicted values match the measured values, then the model is consistent with nature. In addition to predicting phases and their compositions, thermodynamic modeling also predicts the modal amounts of compositional ranges of solid solutions that should crystallize during each particular stage of differentiation. Measured modal amounts of compositional ranges of solid solutions in zoned crystals can be compared with predicted values to further test the validity of thermodynamic models.

Problems associated with estimating modes of zoned crystals include automating the collection of analytical values on zoned crystals and evaluating the error in the estimation of the modal value. In this paper, we address these problems.

AUTOMATION OF DATA COLLECTION

Electron-microprobe analyses provide mineral compositions. The electron microprobe can also be programmed to provide precise, simultaneous estimates of the compositions of zoned minerals and the areas of compositional zones exposed on the surface of a thin section. We have combined an automated program of analytical data collection with a program that processes the analytical data and retains the spatial coordinates for each analytical spot collected on the crystal.

Automated analyses of phenocrysts or microphenocrysts can be done on a grid with a step size chosen to reflect the width of compositional zones in the crystal to be analyzed. The program provides for the selection of step-size and counting time per spot. We commonly use steps in the 10–20 μm range and count for 10 seconds per spot on an ARL, 9-channel, wavelength-dispersion SEMQ electron microprobe to analyze and point-count zoned crystals. The quality of the analyses and of the resulting mode depends on the quality of the polished surface, the grid spacing compared to the width of the composition zones, and the flaws, cracks and inclusions in the crystals analyzed.

Method

Analytical data on background and standards are collected using the same operating procedures as used for regular quantitative analyses (Nicholls & Stout 1986). The operator can collect as many spots on the crystal as is prudent before restandardizing, generally not leaving more than an hour between standardizations. This number of spots (~325) is communicated through the program as the number of spots taken between standardizations, thereby bracketing each group of analyses with appropriate standards. Data reduction, with Bence–Albee corrections, results in a final analysis for each spot. Our off-line data-reduction program also calculates detection limits and precision [see Nicholls & Stout (1986) for equations used]. The precision associated with 10-second counts is obviously less than that for the 20-second counting times normally used. However, the precision on 10-second counting times is sufficient to detect compositional changes in zoned crystals where small step-sizes are used on large phenocrysts. Typical precisions (1σ, in wt%) with 20-second counting times on spots selected by the operator are: SiO_2 0.35%, Al_2O_3 0.30%, FeO 0.11%, MgO 0.17%, CaO 0.05%, Na_2O 0.4%, and K_2O 0.01%. With 10-second counting times on spots automatically located on a grid, typical precisions (1σ, wt%) for oxides in olivine are: SiO_2 0.515%, FeO 0.225%, and MgO 0.196%. The last two are equivalent to 0.32 mol% Fa and 0.34% Fo. For oxides in feldspars the precisions are: SiO_2 0.630%, Al_2O_3 0.438%, CaO 0.049%, Na_2O 0.075%, and K_2O 0.019%. The equivalent precision on the feldspar end-members is: 0.24% An, 0.63% Ab, and 0.10% Or. A typical thermodynamic model for a basaltic bulk-composition calculates a path of crystallization involving compositional changes in mineral and melt in steps of 5°C. Temperature steps of this size correspond to changes of approximately 0.65% Fo and 1.25% An.

The program makes an initial pass through the refined data to eliminate spots collected at grid locations underlain by holes, cracks, or intergrowths of phases with sectional diameters smaller than the diameter of the electron beam, that have oxide totals less than a critical value, *e.g.* <95 wt%. Next, each spot in the set of data is identified as the site of an analysis of a particular mineral. The criteria used to identify minerals are critical values for the range of oxide concentrations. For example, feldspars in a basalt can be uniquely identified if Al_2O_3 concentrations are between 15 and 33 wt% and Na_2O concentrations are between 2 and 13 wt%. The data are further examined for unacceptable analyses by checking the stoichiometry of each composition. If the mineral composition can be expressed as the sum of simple end-members, the sums of the weight percentages of the end members are checked for acceptable totals. Examples are feldspar, olivine and garnet. If the composition cannot be expressed as a set of simple end-members, for example pyroxenes and amphiboles, sums of cations in structural formulas are used in place of end-member totals. Totals outside a chosen range (*e.g.*, a minimum

of 98 to a maximum of 102 wt% end-member totals) indicate a poor analysis, and the analytical data for that spot are eliminated from the data set.

Results of all spot analyses are plotted on a grid using their spatial locations recorded during the microprobe session. Results of each spot analysis, including end-member totals and mineral formula, and its spatial coordinates, are accessible on the computer screen. Analytical data-sets are grouped into compositional ranges based on the amounts of the oxide selected for display (*e.g.*, CaO for feldspar), and the number of spots in each group is tallied (Fig. 1).

Because the analytical mode must be collected on a grid, and most crystals are randomly oriented within the thin section, *i.e.*, are not oriented parallel to the grid and do not have perfectly rectangular or square shapes, most crystals cannot be enclosed exactly within the grid. The outlying spots at which data were collected during the microprobe session must be eliminated. For example, analyzed groundmass feldspar must be excluded from the data file for the chosen target crystal if this crystal is a feldspar. This operation can be done by using the spatial coordinates and comparing the computer image with the microscope image to locate irregular edges. Figure 1A shows a plot of the raw, untrimmed data collected on a plagioclase crystal; Figure 1B, a plot of the trimmed data, shows only data collected on the crystal itself.

The unshaded spots inside the crystal margins correspond to spots at which analyses were made on inclusions in the crystal, *e.g.*, inclusions of magnetite–ulvöspinel solid solution. These compositions will fall outside the acceptable ranges of oxides given for the identification of spots on the target mineral, because those oxide values are specifically chosen to exclude anything but the target mineral, *i.e.*, feldspar in this case. They are, however, accessible, and can be plotted separately. For example, plotting FeO would clearly show the magnetite–ulvöspinel present in or around the feldspar crystal. When locating and isolating the target crystal from groundmass and other crystals, the operator can look at all spots, including unidentified spots.

Each spot marked with an X on Figure 1 indicates the site of an analysis that is definitely a feldspar but falls outside the acceptable analytical range for total wt% oxides or total wt% end members for olivine, feldspar, or garnet; it is not a good quantitative analysis. Only those final values that are acceptable are then included in the numbers of spots of each composition in the crystal.

The program initially divides the total compositional range into bins of equal size on the basis of the complete range in wt% of the selected oxide. However, the operator can adjust the scaling factors used to delineate the bins, and the oxide values can be any equal size when set by the operator after the results are viewed. For example, a 3σ precision value can be used to reflect the compositions that can be differentiated with 99% certainty. The differences in shading correspond to the measured compositional ranges shown in the legend for the crystal.

Example

The Nisga'a (formerly Aiyansh) lava flow north of Terrace, British Columbia, is approximately 22 km long, has a volume close to 0.5 km^3, and contains approximately 14% total iron as FeO. The rocks are almost wholly crystalline, with groundmass crystals ranging in size from 1–2 μm to 25 μm in various samples. A few phenocrysts of olivine (Fo_{64}) and plagioclase (An_{52}) are as large as 1 mm. Scattered pyroxene and plagioclase megacrysts up to 10 mm occur throughout the flow. The Nisga'a lava flow formed from one of the last volcanic eruptions in the Canadian Cordillera, according to accounts by native peoples, radiocarbon dates (1700 AD: Sutherland Brown 1969; 1700 and 1325 AD: Wuorinen 1978), and paleomagnetic dates (1650 AD: Symons 1975). Wuorinen (1978) postulated at least two eruptions, separated by 375 years, in view of the radiocarbon dates.

A thermodynamic model of a crystallization path for a melt with the composition of a sample from the Nisga'a flow was constructed with the MELTS database (Ghiorso & Sack 1995). At 0.3 GPa, the model predicts saturation with olivine ($Fo_{68.3}$) at 1155°C. If a fractional crystallization path was followed, olivine should be joined by plagioclase ($An_{52.5}$) at 1135°C. Olivine and plagioclase fractionate together and change composition as temperature falls. The compositions of the minerals and melt were calculated for each 5° drop in temperature. The mineral compositions in the rock, determined by routine electron-microprobe analyses, are similar to the predicted mineral compositions (Table 1). Table 1 shows a comparison between predicted and measured compositions of the minerals. In general, the compositions of cores and the interiors of the phenocrysts match compositions predicted to crystallize at higher temperatures. The compositions of the rims of the phenocrysts and groundmass grains match compositions predicted to crystallize at lower temperatures. This is the pattern expected if the Nisga'a magma crystallized along a path of simple crystal-fractionation. Consequently, the simple fractionation model might be a viable hypothesis. If the model correctly represents the path of crystallization, then we can infer magmatic temperatures from mineral compositions. However, if the model is incorrect, such inferences are unwarranted. To further test the thermodynamic model, measured amounts of compositional ranges in the phenocrysts can be compared with amounts predicted by the model.

A reasonably straightforward mechanism is to compare relative-cumulative-frequency curves of the measured and predicted compositions. The shapes of

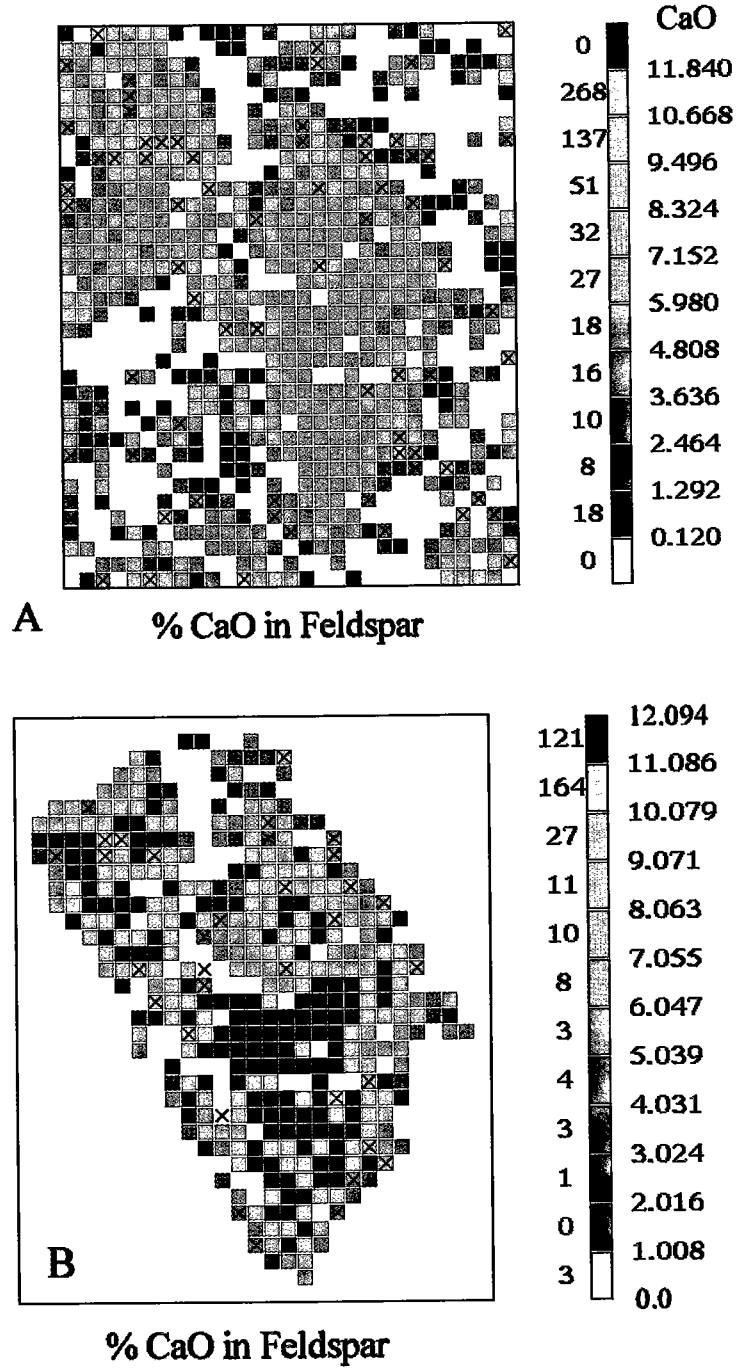

FIG. 1. Maps of results of electron-microprobe analyses for oxides in feldspar, olivine, and garnet. The left columns of numbers in the legends show the number of spots in each compositional range for the oxide. The compositional ranges for the oxides are the column of numbers to the right of the color strip. A. All acceptable feldspar compositions, including groundmass. Shading is related to concentration of Ca. The "X" symbol indicates an analysis that failed to meet the criteria for acceptance (see p.1312). B. Same crystal as A, but with compositions of groundmass feldspars removed. Shading represents different CaO contents. Equivalent An concentrations shown on separate scale. C. Map of MgO concentrations in olivine. Fo concentrations shown with separate scale. D. Map of MnO zoning in garnet. E. Map of MgO zoning in garnet. Same crystal illustrated in D.

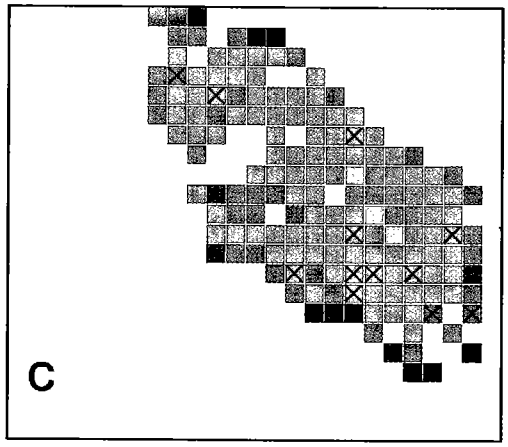

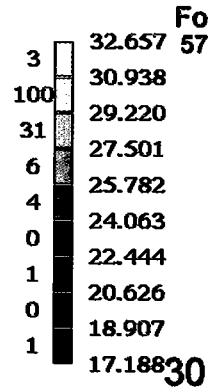

% MgO in Olivine

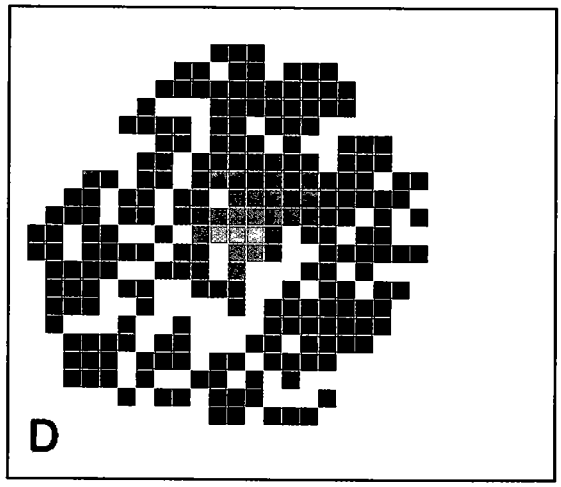

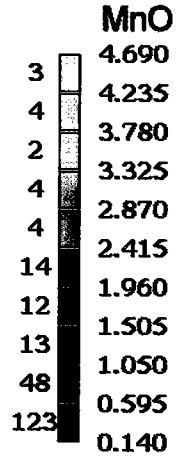

% MnO in Garnet

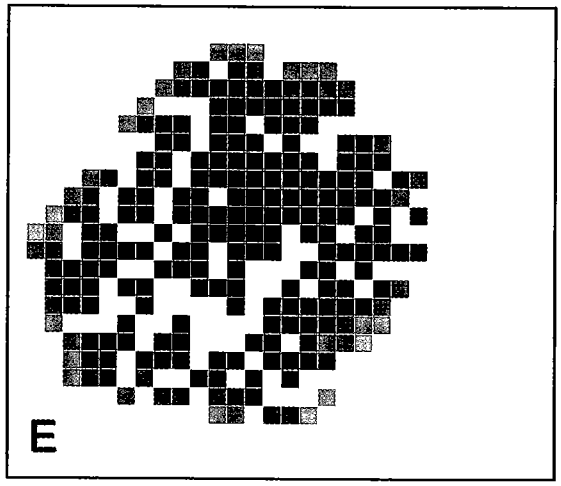

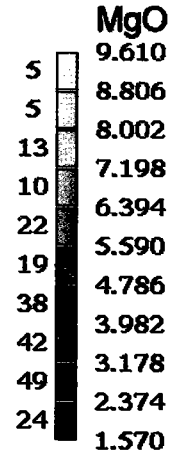

% MgO in Garnet

TABLE 1. CHEMICAL COMPOSITION (wt%) OF NISGA'A FLOW (NR4) AND COMPARISON BETWEEN PREDICTED MODEL COMPOSITIONS AND MEASURED OLIVINE AND PLAGIOCLASE COMPOSITIONS (mol%)

Analysis		T° C	Predicted Fo	Measured Fo	Predicted An	Measured An
SiO_2	46.80	1155	68.3	-	-	-
TiO_2	3.71	1150	67.6	-	-	-
Al_2O_3	14.53	1145	67.0	-	-	-
Fe_2O_3	1.52	1135	65.7	-	52.5	52.5 (c)
FeO	13.52	1130	64.4	63.9 (c)	51.4	51.2 (m)
MnO	0.23	1125	62.9	63.0 (m)	49.8	49.8 (r)
MgO	4.58	1120	61.4	61.3 (m)	48.2	48.2 (r)
CaO	7.58	1115	59.9	60.1 (r)	46.7	46.7 (r)
Na_2O	4.49	1110	58.3	58.4 (m)	45.2	45.4 (g)
K_2O	1.67	1105	56.7	56.7 (m)	43.7	44.2 (r)
P_2O_5	1.18	1100	55.1	55.2 (r)	42.2	42.3 (g)
H_2O^+	0.18	1095	53.3	53.2 (r)	40.4	39.7 (g)
		1090	51.4	51.3 (g)	38.6	38.9 (r)
		1085	49.5	49.5 (r)	36.7	36.7 (g)

(c) = core of crystal; (m) = middle; (r) = rim; (g) = groundmass

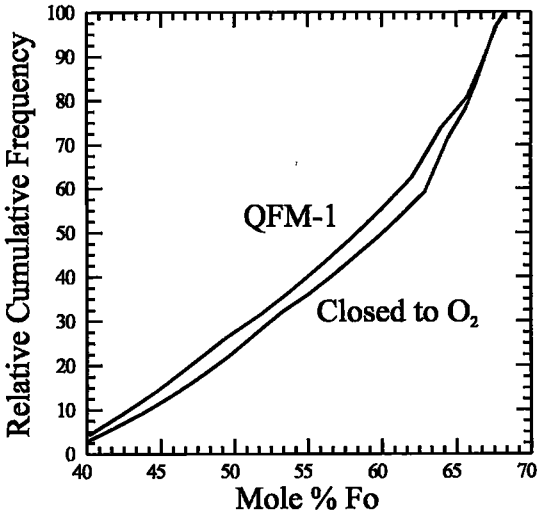

FIG. 2. Relative-cumulative-frequency curves for two thermodynamic models for the fractionation of a Nisga'a basalt at 0.3 GPa. QFM – 1 is the fractionation path for olivine compositions and amounts, with fugacity of oxygen constrained to one log unit below the Quartz – Fayalite – Magnetite buffer. The path that the same melt would follow if fugacity of oxygen was constrained by the ferrous–ferric ratio of the rock is labeled Closed to O_2.

these curves are model-dependent, *i.e.*, the curves are different for different conditions of crystallization such as pressure, H_2O content, and oxygen fugacity; this feature is indispensable, because models could not be differentiated if every model produced the same relative-cumulative-frequency curve. Figure 2 illustrates the curves displaying the olivine compositions that should crystallize from the Nisga'a melt under different

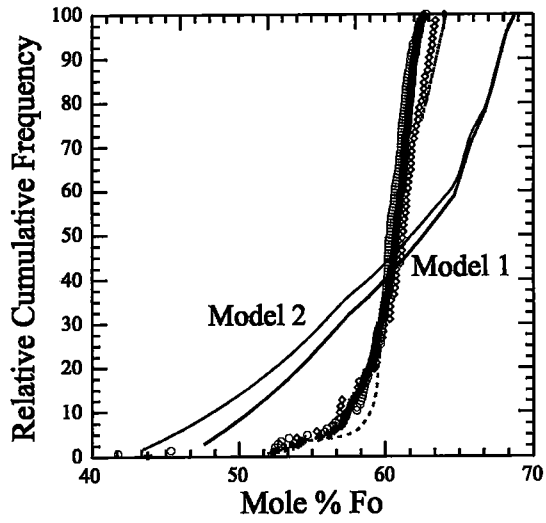

FIG. 3. Relative-cumulative-frequency curves for compositions measured on grids on near-central sections through three phenocrysts of olivine from a basalt. The model curves were derived from the volumes of olivine compositions predicted to crystallize from fractionating melts with the initial composition of basalt. Model 1 represents an isobaric path at 0.3 GPa. Model 2 represents a fractionation path at 0.3 GPa, followed by eruption to the surface at the stage of saturation with K-rich feldspar. Open circles, diamonds, and crosses represent data points from three different crystals. Dashed curves are exaggerated, schematic illustrations of the changes to the relative cumulative curves if corrected for systematic error in the area-to-volume conversions. The real corrections are too small to show at the scale of the diagram.

conditions of oxygen fugacity. One thermodynamic model was run with the oxygen fugacity set to one log unit beneath the Quartz – Fayalite – Magnetite (QFM – 1) buffer and the other model was closed to O_2; the oxygen fugacity was buffered by the Fe^{2+}:Fe^{3+} ratio of the rock. The relative-cumulative-frequency curves are clearly distinct (Fig. 2).

The relative-cumulative-frequency curves for spots collected on three olivine phenocrysts from the Nisga'a flow are shown on Figure 3. The crystals were selected because the highest Fo contents measured were found at their cores. Plotted, for comparison, are the relative-cumulative-frequency curves for two thermodynamic models, both at QFM – 1. One model is a fractionation model at constant pressure. The second model describes a two-stage path of crystallization with eruption at the surface as a second stage. Figure 4 is a similar plot for four feldspar phenocrysts. There are marked differences between the curves generated from model predictions and the curves derived from the data for both olivine and feldspar.

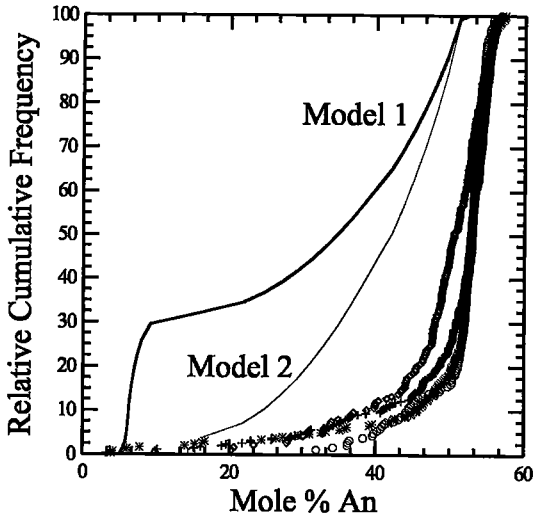

FIG. 4. Relative-cumulative-frequency curves for compositions measured on grids on near-central sections through four phenocrysts of plagioclase from the same basalt that crystallized the olivine whose data is displayed in Figure 3. The model curves were derived from the volumes of plagioclase compositions predicted to crystallize from fractionating melts with the initial composition of the basalt. Model 1 represents an isobaric path at 0.3 GPa. Model 2 represents a fractionation path at 0.3 GPa, followed by eruption to the surface at the stage of K-rich feldspar saturation. Open circles, diamonds, stars, and crosses represent data points from the four different crystals.

These techniques for collecting the data and the methods of displaying them provide an efficient way to compare the patterns of zoning of different elements in the same crystal. Figure 5 shows marked differences in the cumulative frequency distributions for MnO and MgO in a garnet from the granulite facies, Pitka Complex, Alaska (E.D. Ghent, pers. comm.). The differences in slope of the frequency distributions show that Mn decreases in concentration rapidly from center to edge of the crystal. Magnesium, in contrast, increases in concentration more evenly from center to edge.

DISCUSSION

Two aspects of the mechanism for comparing model-derived and measured relative-cumulative-frequency curves require discussion before the differences can be used as evidence that the model provides an inadequate hypothesis for the path of crystallization for the rock. The first concerns a method or procedure for deciding whether or not two cumulative curves are sufficiently different to be significant. The second aspect focusses on whether or not the frequencies with which spots within a compositional range are measured on a surface cut through a crystal reflect the relative volumes of the compositional ranges in that crystal.

The Kolmogorov–Smirnov test (K–S test) has been used to determine whether two relative-cumulative-frequency distributions are significantly different (Press *et al.* 1992). The test determines whether or not the largest difference in frequency between two

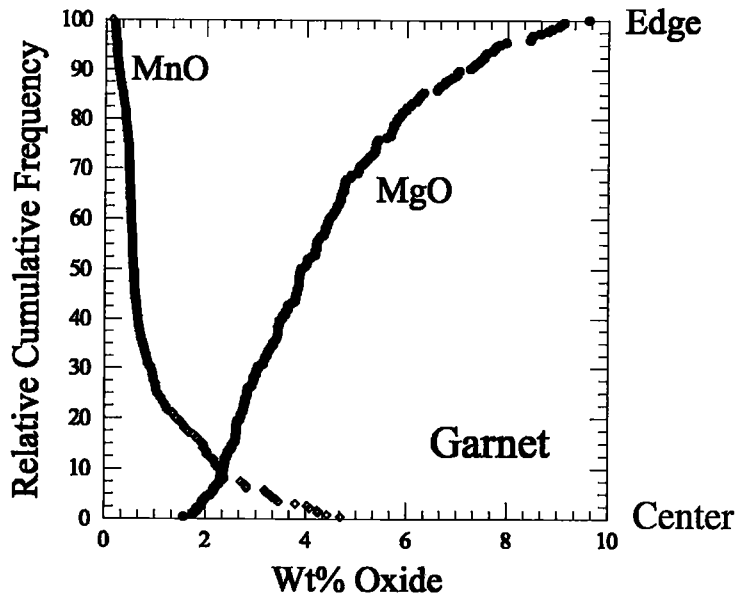

FIG. 5. Mn and Mg zoning profiles in a garnet porphyroblast in a granulite-facies gneiss from Alaska. Circles represent Mg concentrations (expressed as MgO), whereas diamonds represent Mn concentrations (expressed as MnO).

distributions is likely to happen by chance. The test, however, is so strongly dependent on the number of data points used to construct the curves that any difference between the curves, no matter how small, will return a result that indicates the existence of a significant difference if the number of data points is large. If the number of data points is even a few hundred, two cumulative curves derived from two modes measured on the same crystal would be considered significantly different. Other tests are modifications of the K–S test and use the same parameters. Consequently, there does not appear to be a satisfactory statistical test for distinguishing different cumulative curves. We are left with making a judgement based on experience.

The ability to reject false hypotheses because the volume–composition relationships in a rock or crystal do not fit a model that predicts such relationships depends, in part, on the accuracy of the volume estimates of the constituents in the rock or crystal. Any section through a rock or crystal can provide estimates of the volumes of the phases or compositions that make up the rock or crystal. These estimates are derived from measured areas exposed on the surface of the section. The fractional areas of the constituents exposed on a section through a composite solid are equivalent, in a statistical sense, to the fractional volumes of the consituents. However, areas in sections through composite solids can, at best, be only estimators of the volumes. The central problem is to evaluate the quality of the estimate. The only statement in the literature that addresses this problem is Chayes's (1956) demonstration that the fractional areas underlain by the constituents in any section are consistent estimators of the volumes of the constituents in the rock or crystal. Chayes (1956) also discussed the effects of regular arrangements of the constituents in banded rocks on volume estimates, where he demonstrated the consistent nature of the fractional areas in section as estimators of the fractional volumes of the constituents. Oriented constituents and regular arrangements do not invalidate the consistent property of sectional areas as estimators of fractional volumes, but oriented and regular arrangements do create sampling problems.

A detailed discussion of the effects of concentric zoning on the estimation of fractional volumes from fractional areas in sections through crystals is provided in the Appendix. The principal conclusions follow.

Central sections (sections cut through the center of the crystal)

1. The areas of outer shells will underestimate the volumes of the shells, *i.e.* the fractional areas exposed on central sections are smaller than the fractional volumes of the shells (Fig. 6).
2. The fractional areas of inner shells overestimate the fractional volumes of the shells (Fig. 6).
3. The maximum error of estimation, as a percentage of the total volume of the crystal, is approximately 15%. If the outer shell has a thickness equal to one-third the dimension of the crystal, or if the inner core has a thickness equal to two-thirds the dimension of the crystal, then the estimated volume will be in error by 15%. It is important to realize that this error is systematic and not random. The volume cannot be in error by ±15%; rather the volume of the outer shell will be underestimated by 15%, and the volume of the core will be overestimated by 15%. Also, if the shells are thinner or thicker, the error will be less (Fig. 6).
4. The systematic errors that arise from estimating fractional volumes from fractional areas in section decrease with decreasing thickness of the shells.
5. Shells that have a width centered approximately two-thirds the distance from the center to edge of the crystal will have minimal (~0%) systematic error in their estimated volumes.

Non-central sections

6. For any given shell, there is at least one section in which the fractional area of the shell equals the fractional volume of the shell (Fig. 7).
7. One section cannot provide fractional areas that are perfect estimators of volumes for all shells.
8. In theory, a large number of sections through a crystal could be cut, and fractional volumes could be estimated from the fractional areas. The average of those estimates would approximate the volume, because there are sections that provide both positive and negative errors, a reflection of the consistent nature of the process of estimating volumes from areas.

Consequences

Points 1 and 2 above have particular consequences in a comparison of model-derived and measured cumulative curves for centrally sectioned crystals. If the relationships shown in Figure 3 are appropriate for normally zoned crystals of olivine, then the systematic errors can only cause the differences between the curves to be smaller at the high end and larger at the low end. The true volumes of Fo-rich cores and inner shells are underestimated; consequently, the volume of compositions between Fo_{60} and Fo_{70}, say, must be larger. Because the data are normalized to 100%, the data points near Fo_{60} must be at a smaller cumulative percentage. Concurrently, the true volumes of the Fo-poor zones are smaller than the estimates. Consequently, the Fo-poor compositions must plot at smaller values on the cumulative axis so that the volumes of the Fo-poor zones are smaller. If the model-measured relations shown on Figure 4 characterize a mineral, then the systematic errors can only weaken the agreement if the crystal is normally zoned. In addition, the curves can shift by a maximum of 15%; usually the shift will be much less because shells and cores generally are thin.

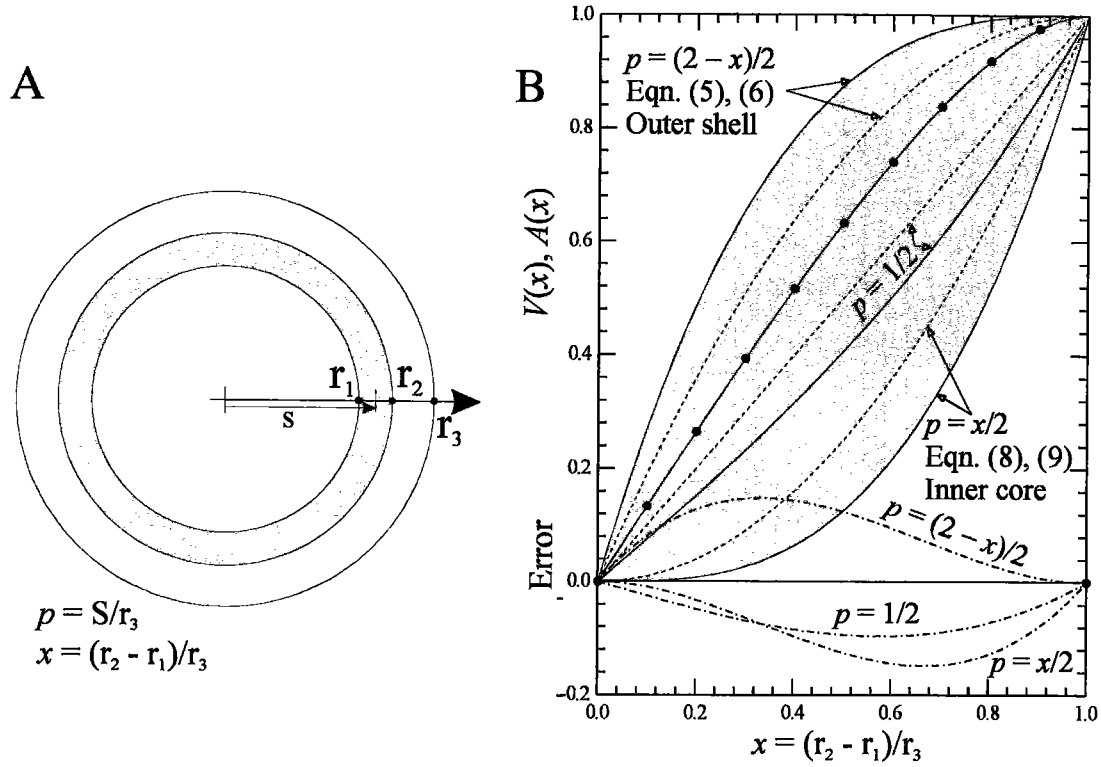

FIG. 6. A) Sketch of a concentric shell in a central section through a spherical crystal. B) Plots of fractional volumes, $V(x)$, of concentric shells and fractional areas, $A(x)$, underlain by shells in central sections against thickness of the shell (x). Volumes are shown with solid lines, areas with dotted lines. Errors arising from estimating volumes from areas are shown with dash–dot lines. The curve with solid dots marks sections where the estimated volumes equal the areas.

The compositional zones in the crystals that supplied the data for Figures 3 and 4 are thin, approximately one-tenth of the crystal's thickness or less, and the curves would shift by much less than 15%. The directions of the shifts are shown schematically on Figure 3 (dashed curves).

The differences between relative-cumulative-frequency curves for models and crystals shown on Figures 3 and 4 are too large to ascribe to systematic errors in the estimates of the fractional volumes of the compositional zones. Consequently, the crystallization models postulated for the rock are incorrect. The remarkable similarities between the relative-cumulative-frequency curves for several crystals of olivine and of feldspar in the rock indicate that all the crystals in each set of minerals coprecipitated and recorded similar, albeit unknown, conditions. The similarities amongst these crystals justify the use of relative volumes estimated from the cumulative frequency curves to test hypotheses.

CONCLUSIONS

Although concentrically zoned crystals have no sections that provide exact estimates of fractional volumes from fractional areas for all shells, the direction and amount of the systematic error introduced can be estimated. For crystals with thin compositional shells, the systematic error is small enough to eliminate most, if not all, incorrect models of crystal growth in rocks. The easiest sections to interpret are central sections through crystals. Although the methods outlined in this paper were developed for the determination of analytical modes with the electron microprobe, the geometric constraints on the relationship between fractional volume and fractional area are independent of the method of measuring the modes.

The compositions and amounts of the measured areas in sections through concentrically zoned crystals can be compared to the thermodynamically predicted compositions and amounts. If the match is good, it

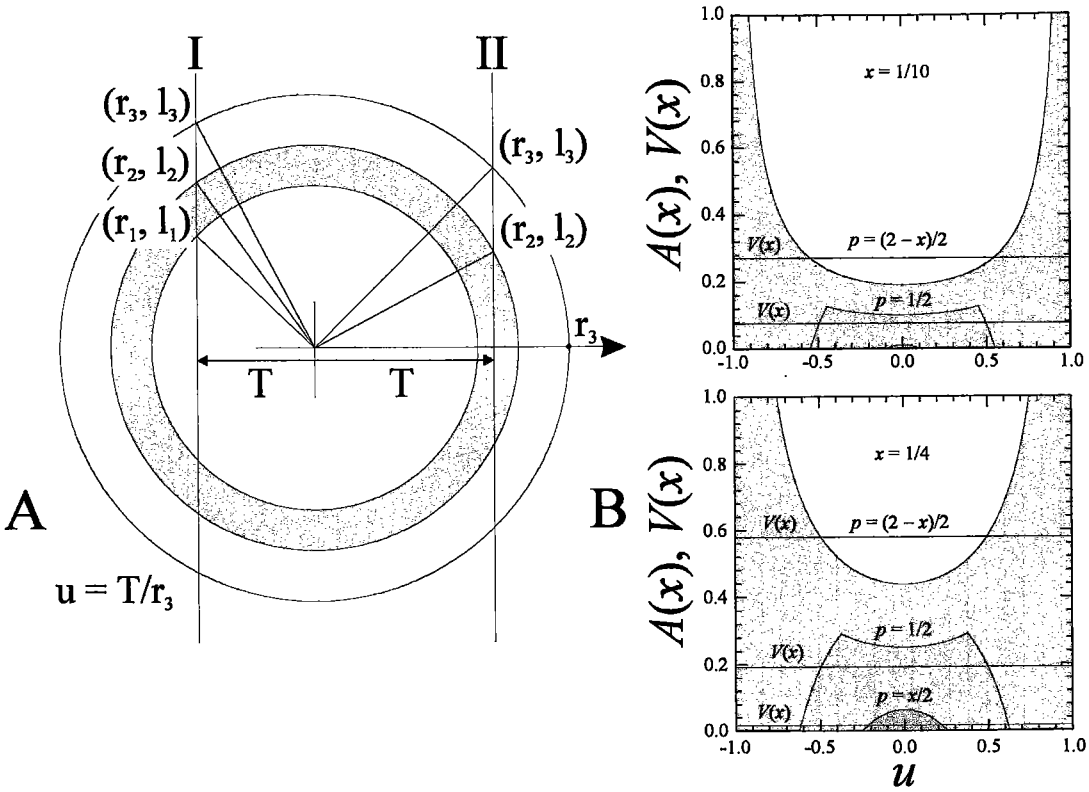

FIG. 7. A) Sketch of a concentric shell in non-central sections through a spherical crystal. The sections are cut normal to the plane of the paper, and two traces are shown, I and II. B) Plots of fractional volumes, $V(x)$, of concentric shells, and of fractional areas, $A(x)$, underlain by shells in non-central sections against fractional distance of the shell (u) from the center of the crystal. Upper diagram is for a thin shell with a thickness one-tenth that of the crystal. Lower diagram is for a thicker shell with a thickness one-quarter that of the crystal. The volumes for an outer shell [$p = (2 - x)/2$], one half way between center and edge [$p = ½$], and an inner core [$p = x/2$] are shown with solid horizontal lines.

provides permissive evidence that the postulated path of crystallization could be the real path. In cases of disagreement between the model and measured values, the measured values may suggest a different scenario, *e.g.*, perhaps the process is two-staged, and the magma resided for some time part way to the surface, allowing the crystals more time for growth at an approximately constant composition of the melt, rather than moving directly up and out. The physical conditions influencing the processes of formation should be reflected in the amounts of early compositions in phenocrysts in the rock. This is illustrated by the similarity of three olivine and four feldspar crystals in the Nisga'a flow.

This method of collecting analytical modes could be used for additional discretionary testing in any problem relating one rock to other rocks (melts) or to a postulated source-composition. It should be applicable in most research that uses mass balances based on mineral compositions and the modal amounts of each composition. If one postulated a reaction relationship in a study of compositional zoning, this method, which gives both mass and compositional data, will provide more than just an accurate picture of the compositional zones. For example, a sample from the Bonnington Pluton in British Columbia contains orthopyroxene, clinopyroxene and amphibole in a reaction relationship. Knowledge of the relative amounts of the compositions, as well as of the amounts of the phases, would place constraints on the reaction path that was frozen into the rock. In process-oriented studies, a significantly greater amount of a particular composition may suggest more time for growth at that particular set of physical conditions. Using a known or theoretically estimated growth-rate, a calculation of residence time could be made. This method of precise analysis of compositional zoning could also provide information useful to any study of zoning processes. As an example, Figure 5 illustrates Mg and Mn zoning in a garnet from a gneiss

in the Pitka Complex, Alaska. This crystal of garnet is from a high-pressure granulite-facies rock and records pressures in excess of 1.0 GPa (E.D. Ghent, pers. comm.). The pattern of zoning, if related to changes in pressure, indicates increasing pressure with growth.

Acknowledgements

The Natural Sciences and Engineering Research Council of Canada (NSERC) supported this work through research grant 7232 and Lithoprobe grants. Dr. Daniel Barker, The University of Texas at Austin, provided comments and criticism that led us to develop the geometrical analysis in the Appendix. J.K. Russell, H. Jamieson, and G.T. Nixon provided excellent and constructive reviews. Any lapses in logic and lack of clarity are ours, not theirs.

References

Chayes, F. (1956): *Petrographic Modal Analysis – An Elementary Statistical Appraisal.* John Wiley & Sons, Inc., New York, N.Y.

Ghiorso, M.S. & Sack, R.O. (1995): Chemical mass transfer in magmatic processes. IV. A revised and internally consistent thermodynamic model for the interpolation and extrapolation of liquid–solid equilibria in magmatic systems at elevated temperatures and pressures. *Contrib. Mineral. Petrol.* **119**, 197-212.

Nicholls, J. & Stout, M.Z. (1986): Electron beam analytical instruments and the determination of modes, spatial variations of minerals and textural features of rocks in polished section. *Contrib. Mineral. Petrol.* **94**, 395-404.

Press, W.H., Teukolsky, S.A., Vetterling, W.T. & Flannery, B.P. (1992): *Numerical Recipes in FORTRAN, The Art of Scientific Computing.* Cambridge University Press, Cambridge, U.K.

Sutherland Brown, A. (1969): Aiyansh lava flow, British Columbia. *Can. J. Earth Sci.* **6**, 1460-1468.

Symons, D.T.A. (1975): Age and flow direction from magnetic measurements on the historic Aiyansh flow, British Columbia. *J. Geophys. Res.* **80**, 2622-2626.

Wuorinen, V. (1978): Age of Aiyansh Volcano, British Columbia. *Can. J. Earth Sci.* **15**, 1037-1038.

Received November 5, 1996, revised manuscript accepted August 7, 1997.

Appendix

Volumes estimated from areas

Estimates of the fractional volumes of compositional ranges in crystals are complicated by concentric patterns of zoning and by the selection of sections that cut through the center (or close to the center) of the crystal. In this section, we examine the errors in estimates of fractional volumes from fractional areas (see Figs. 6 and 7) in central and non-central sections cut from concentrically zoned crystals.

If an orthogonal crystal with sides a_2, b_2, c_2 contains an inner core with sides a_1, b_1, c_1, and maintains a constant aspect-ratio during growth, then the relationships between the sides of the crystals and the core are given by:

$$a_2 - a_1 = x\, a_2 \quad (1)$$

$$b_2 - b_1 = x\, b_2 \quad (2)$$

$$c_2 - c_1 = x\, c_2 \quad (3)$$

where x is the fractional width of the outer shell. Note that x is the same for all three edges, but that the absolute width of the outer shell is different on the different bounding surfaces, a consequence of the constant aspect-ratio.

The fractional volume of the shell outside the core is given by:

$$V(x) = (a_2b_2c_2 - a_1b_1c_1)/(a_2b_2c_2) \quad (4)$$

Substitution of the relations given in Equations (1) – (3) into Equation (4) produces the result:

$$V(x) = x^3 - 3x^2 + 3x \quad (5)$$

where $V(x)$ is the fractional volume of the outer shell as a function of the thickness of the outer shell, x, expressed as a fraction of the total length of the crystal edges.

Central sections

The fractional area, $A(x)$, of an outer shell in a central section (a section cut through the center of the crystal) as a function of the thickness of the outer shell expressed as a fraction of the total length of the crystal edges, x, is:

$$A(x) = x(2 - x) \quad (6)$$

Equations (5) and (6) are valid for spheres and cubes as well as rectangular parallelepipeds that maintain the same aspect-ratio during growth. The appropriate dimension for spherical shapes is the radius. Cube-shaped crystals and rectangular parallelepipeds must also be

cut parallel to one side of the crystal for Equation (6) to hold. The applicability of the same equation to several solids with different shapes means that treating the crystal as a sphere will provide general information about the effects expected for sections through concentrically zoned crystals. Equations (5) and (6) are plotted on Figure 6 and carry the label $p = (2 - x)/2$, where p is the fractional distance of the shell from the center of the crystal. Equation (5) is represented by a solid line, and Equation (6) is shown with a dashed line.

The difference between the fractional volume of an outer shell and the fractional area of that shell in a central section [Equation (5) minus Equation (6)] is the error that results from using areas as an estimator of volumes. An equation explicitly expressing the error (Δ) is given by:

$$\Delta = x(x^2 - 2x + 1) \quad (7)$$

Equation (7) is also plotted on Figure 6 as a dash–dot line labeled $p = (2 - x)/2$.

The fractional volume, $V(x)$, of an internal shell in a crystal is a function of the thickness of the shell, expressed as a fraction of the total thickness of the crystal, and the position of the shell between the center and outer edge of the crystal, p (Fig. 6):

$$V(x) = x(x^2 + 12p^2)/4 \quad (8)$$

The fractional area in a central section, $A(x)$, of an internal shell in a crystal is also a function of the thickness of the shell, expressed as a fraction of the total thickness of the crystal, and the position of the shell between the center and outer edge of the crystal, p:

$$A(x) = 2px \quad (9)$$

The maximum and minimum values that p can take arise because the shell must have a finite thickness and lie within the crystal. These limits are:

Maximum $= (2 - x)/2$
Minimum $= x/2$

Curves representing Equations (8) and (9) for maximum and minimum values of p, as well as the intermediate value of one-half, are plotted on Figure 6. Solid lines represent the volumes; dashed lines represent the areas.

The values of p, as a function of x, that make $A(x)$ equal to $V(x)$ are given by:

$$p = [\sqrt{(4 - 3x^2)} + 2]/6 \quad (10)$$

The values of the fractional volume that are the same as the values of the fractional area in central sections through a crystal are obtained by substituting the expression for p in Equation (10) into Equation (8). The result is:

$$V(x) = [x(\sqrt{(4 - 3x^2)} + 2)]/3 \quad (11)$$

Equation (11) is plotted on Figure 6, where the resulting curve is marked with large solid circles. This curve relates the volumes of the shells, which can be exactly obtained from measurements of the area of the shell exposed in the central section. Only shells with particular thicknesses and locations can have their volumes exactly estimated from the exposed areas. All other shells will have estimated volumes in error.

The difference (Δ) between the fractional volume of a shell and the fractional area of a shell in a central section depends on the thickness of the shell, x, and its position in the crystal, p:

$$\Delta = x(x^2 + 12p^2 - 8p)/4 \quad (12)$$

At the maximum and minimum values of p, Equation (12) reduces to:

$$\Delta = x\,(x - 1)^2 \text{ and} \quad (13)$$
$$\Delta = x^2\,(x - 1)$$

Equations (12) and (13), with $p = ½$ in Equation (12), are plotted on Figure 6 with dash–dot lines. These curves describe the errors associated with estimating volumes from areas in central sections through concentrically zoned crystals. Volumes of inner shells will be overestimated by measured areas, whereas the volumes of outer shells will be underestimated. If the shells are thin, the cut-off position between under- and overestimation is approximately $p = 2/3$ [*i.e.*, set x equal to zero in Equation (10)]. The largest error is approximately 15% of the total volume of the crystal and occurs in the estimate for an outer shell that has a thickness equal to one-third the thickness of the crystal or occurs in the estimate of an inner core with a thickness equal to two-thirds the thickness of the crystal (Fig. 6).

Generalization to rectangular crystals

Equations (8) and (9) can easily be generalized to a rectangular crystal. Suppose the crystal has edges a_3, b_3, c_3 and a shell with widths given by:

$$a_2 - a_1 = x\,a_3$$
$$b_2 - b_1 = x\,b_3$$
$$c_2 - c_1 = x\,c_3$$

Define the fractional distances of the center of the shell from the crystal's center in the three orthogonal directions parallel to the crystal edges by:

$$p_1 = ½\,(a_1 + a_2)/a_3$$
$$p_2 = ½\,(b_1 + b_2)/b_3$$
$$p_3 = ½\,(c_1 + c_2)/c_3$$

Then the analogues for Equations (8) and (9) are:

$$V(x) = x[x^2 + 4(p_1p_2 + p_1p_3 + p_2p_3)]/4$$
$$A(x) = x(p_1 + p_2)$$

The only restriction is that the section on which the area corresponding to the last equation is measured must be cut parallel to two of the edges of the crystal.

Non-central sections

The fractional area displayed by a concentric shell depends on whether the thin section is inside, within or outside the shell. If the thin section cuts the crystal between the center of the crystal and the inner edge of the shell (Fig. 7A, Section I), the fractional area of the shell exposed on the thin section is given by:

$$A(x) = 2px/(1 - u^2) \quad (14)$$

where the fractional distance of the section from the center of the crystal is represented by u. The limits on u and p, in this case, are:

$$0 < u < (2p - x)/2$$
$$x/2 < p < (2 - x)/2$$

If the section is cut within the shell (Fig. 7A, Section II), then the equation describing the fractional area exposed is:

$$A(x) = [x^2 + 4px + 4(p^2 - u^2)]/[4(1 - u^2)] \quad (15)$$

The limits on u, in this case, are:

$$(2p - x)/2 < u < (2p + x)/2$$

If the section is cut outside the shell, the fractional area is obviously zero:

$$A(x) = 0,\ u > (2p + x)/2 \quad (16)$$

Two examples of Equations (14) – (16) are plotted on Figure 7B. Values of $A(x)$ are plotted as functions of u for fixed values of x and p. The general shapes of the curves are the same for all values of x; they attain different values, depending on x. The curves have different shapes that depend on p. If the shell is an outer shell [$p = (2 - x)/2$], then any section will sample the shell. If the section is within the outer shell, then only the outer shell will be exposed on the surface of the section, and the fractional area will be 1. If the section cuts inside the shell, then the fractional area will be given by the u-shaped part of the curve. Two sections will expose fractional areas equal to the fractional volume. The values of u that characterize these two sections are given by the intersection of the horizontal line labeled $V(x)$ with the u-shaped curve. For the case of a shell at an intermediate location between the center and edge of the crystal ($p = ½$), there is a discontinuity in slope between locations of sections that cut the crystal inside the shell and those that cut through the shell (Section II, Fig. 7A). Again, there are two sections that will expose fractional areas numerically equal to the fractional volume of the shell. If the subvolume of interest is the core of the crystal, then only a section that cuts the core will expose its area at the surface of the section. Also, there are two sections that expose areas numerically equal to the fractional volume of the core. In the case where $x = 1/10$, the line representing the fractional volume plots too close to the x axis to be visible.